Polymer Testing 28 (2009) 746–751

Contents lists available at ScienceDirect

Polymer Testing

journal homepage: www.elsevier.com/locate/polytest

Material Characterisation

The microstructural characterization of PA6/PA12 blend specimens fabricated by selective laser sintering

G.V. Salmoria*, J.L. Leite, R.A. Paggi

CIMJECT, Departamento de Engenharia Mecânica, Universidade Federal de Santa Catarina, UFSC 88040-900 Florianópolis, SC, Brazil

ARTICLE INFO

Article history:
Received 11 May 2009
Accepted 22 June 2009

Keywords:
Selective laser sintering
Microstructure
PA6/PA12 blends

ABSTRACT

This study investigates the processing of blends of polyamide 6 (PA6) and polyamide 12 (PA12) by selective laser sintering (SLS) using a CO_2 laser. Powder properties of undiluted polymers, mixture composition, and processing parameters, as well as their influence on the microstructure of the specimens manufactured, were evaluated. Polyamides showed higher absorption of laser energy during the sintering of blend specimens, with subsequent thermal energy transfer to the melting of the polymeric phases. The structure of parts obtained by SLS is dependent on the process parameters and the characteristics of the powder material to be processed. The microstructures of PA6/PA12 blend specimens were heterogeneous, with co-continuous and disperse phases depending on the quantity of PA12. The porosity and crystallinity also changed as a function of the component proportions. The use of polymeric blends can increase the range of structures and properties of SLS parts.

1. Introduction

The structure and properties of parts to be manufactured by selective laser sintering (SLS) should be considered according to their application. The level of control over the microstructure of SLS parts is dependent on the process parameters, particularly the powder properties [1–6], since these can influence other parameters. For example, particle shape and size distribution influence the powder packing density while the melt flow behavior and the thermal stability define the laser power and scan speed [1,3,4].

The use of polymers in the SLS process can offer some advantages over other materials. However, the variety of commercial polymeric materials available for the SLS process is restricted and this reduces the options available during the material selection for the manufacturing of parts [4–12]. The use of non-commercially available polymers and mixtures of polymers can increase the range of properties of the SLS parts [10–12].

Previous studies have shown that immiscible blends of PA12/HDPE offer an alternative means to obtain SLS parts with specific multiphase structures and properties, permitting the development of new applications [13,14]. This study investigated the powder material properties, mixture composition and processing conditions, as well as their influence on the microstructure of a polar blend system of polyamide 6 and polyamide 12 processed by SLS.

2. Experimental

2.1. Materials

The polymeric powders used in this study were commercial Polyamide 6 (PA6) MAZMID B260 (Mazzafero Tecnopolímeros S.A.) and polyamide PA12 (EOSINT) with average particle sizes of 150 and 60 μm, respectively.

2.2. Selective laser sintering of specimens

The specimens (dimensions: $10 \times 5 \times 3$ mm) of undiluted polymers and mixtures of PA6 and PA12 powders of

* Corresponding author. +55 48 3721 3987; fax: +55 48 3721 7315.
E-mail address: gsalmoria@emc.ufsc.br (G.V. Salmoria).

0142-9418/$ – see front matter © 2009 Published by Elsevier Ltd.
doi:10.1016/j.polymertesting.2009.06.010

80/20, 50/50 and 20/80 (w/w) were processed by SLS using a 20 W RF-excited CO_2 laser (wavelength: 10.6 μm; laser beam diameter: 250 μm). The processing parameters were: layer thickness 150 μm, laser scan speed 44 mm/s and chamber temperature 120 °C. The laser power was 2–3 W, according to the blend composition, as previously defined based on the optimization of the experimental parameters.

2.3. Infrared spectroscopy, differential scanning calorimetry and melt flow measurements

Infrared spectra of the polymers were obtained using a 16 PC Perkin Elmer spectrophotometer, performing 20 scans at a resolution of 4 cm^{-1} using KBr plates, in order to evaluate polymer absorbance at the CO_2 laser wavelength. Differential scanning calorimetry (DSC) curves were obtained using a differential scanning calorimeter (Shimatzu 50) from 25 to 300 °C at a heating rate of 10 °C min^{-1}. The average sample size was 5 mg and the nitrogen flow-rate was 25 cm^3 min^{-1}.

The melt flow index (MFI) were determined at different temperatures (Table 1) and moderate strain-rate using 2.16 kg of static mass in T.Q.-CEAST equipment according to ISO 1133.

2.4. Scanning electron microscopy and X-ray diffraction

The polymer powders and specimens were inspected using a Philips XL30 scanning electron microscope (SEM) in order to investigate their particle aspects, microstructures and cryogenic fracture topographies and features. The specimens were coated with gold in a Bal-Tec Sputter Coater SCD005.

The X-ray diffraction measurements were performed using a Philips PW1150 vertical diffractometer. The Cu–Kα nickel filtered radiation was detected in the range of 6–50 degrees. The results of these analyses were used to control the microstructure of the specimens.

3. Results and discussion

Fig. 1 shows the infrared spectra of PA6 and PA12 from 6.0 to 25.0 μm. At 10.6 μm it is possible to observe an absorption band for the polyamides corresponding to the vibration of amide groups. The presence of absorption at 10.6 μm can be explained by the low amount of laser power needed to process polyamides by CO_2 laser. PA12 has a lower melting temperature than PA6, as revealed by the DSC curves (Fig. 2). The melting temperatures and enthalpies obtained for PA6 and PA12 were 220 °C and 68 J g^{-1}, and 178 °C and 46 J g^{-1}, respectively.

Table 1
Melt flow index of PA6 and PA12 at different temperatures.

	Temperature (°C)	MFI (g/10 min)
PA6	230	23.2
	260	38.3
	278	45.8
PA12	200	2.38
	230	17.9
	260	41.8

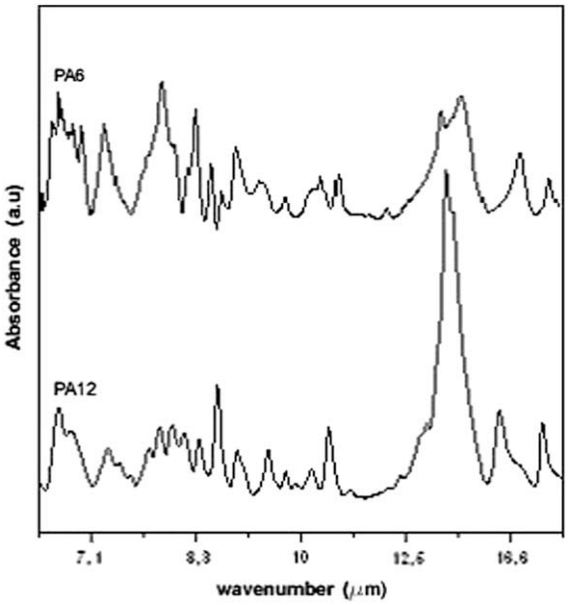

Fig. 1. Infrared spectra for PA6 and PA12.

PA6 and PA12 with average sizes of 150 and 60 μm, respectively, had irregular particle shapes as shown in the powder micrographs (Fig. 3a and b). With the processing parameters used in the SLS, the PA6 specimen surface showed a higher degree of sintering, with particles joined by extensive co-continuous phase formations, as can be observed in the micrographs shown in Fig. 3c and e. The surface of pure PA12 sintered specimens (Fig. 3d and f) had an evident neck formation mechanism and there was a homogeneous distribution of interconnected pores with the average size being related to the particle size and shape of the original powder.

Fig. 4 shows the X-ray diffractograms for the PA6 and PA12 powders and sintered specimens. Polyamides can crystallize into more than one crystal structure with different chain folding patterns which influence the mechanical properties. The alpha phase (monoclinic or triclinic) is the usual phase found for polyamides with a low

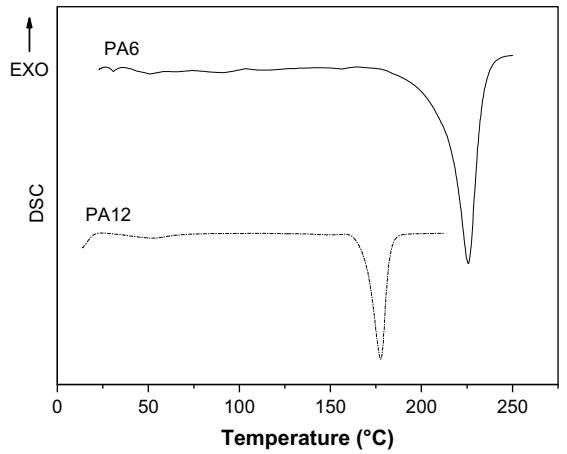

Fig. 2. DSC curves for PA6 and PA12 powders.

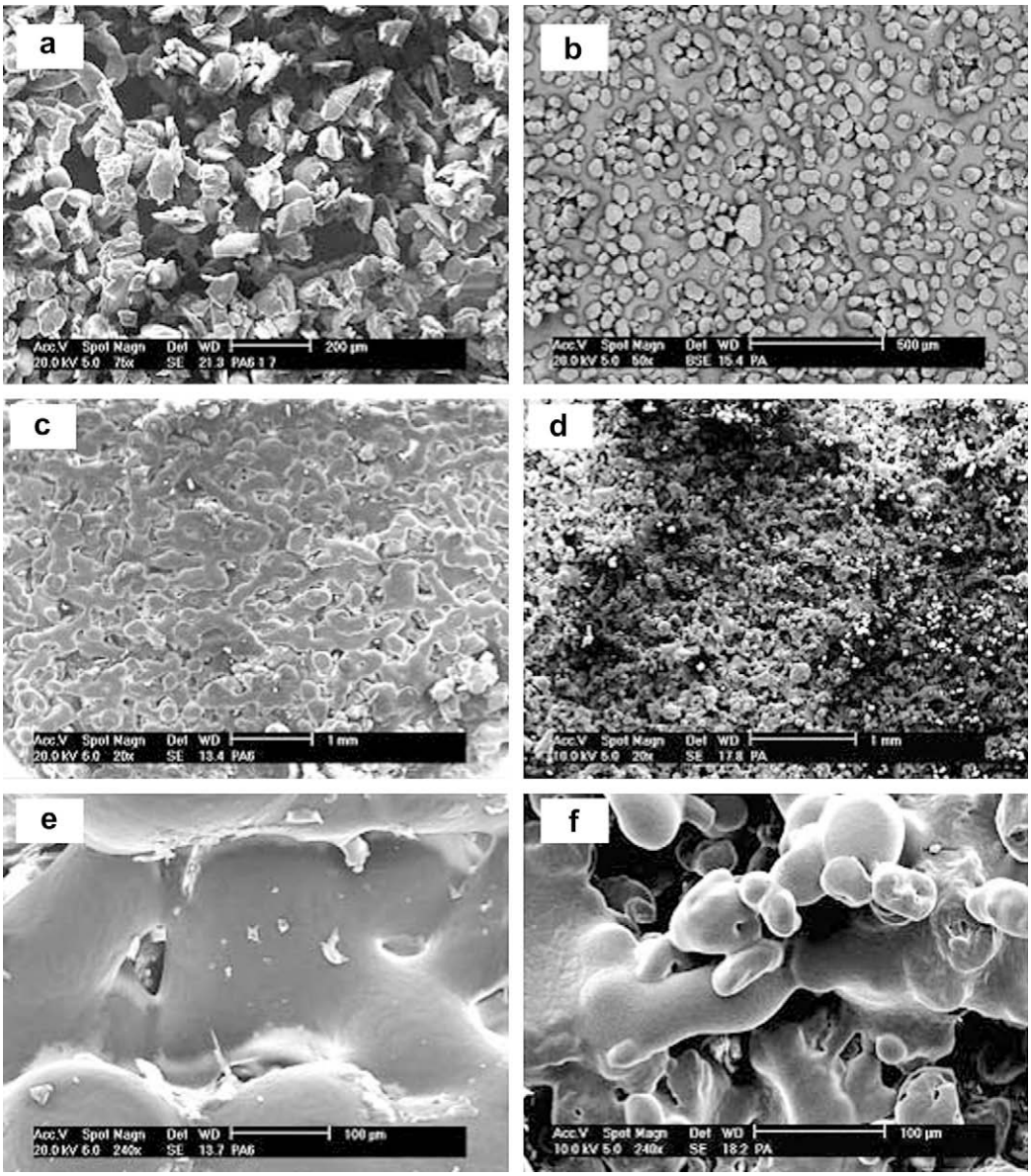

Fig. 3. Micrographs for: (a) PA6 powder, (c) and (e) PA6 specimen 20× and 240× magnification, respectively, (b) PA12 powder, and (d) and (f) PA12 specimen 20× and 240× magnification, respectively.

number of methylene units. The gamma phase (pseudo-hexagonal) is found in polyamides with a larger number of methylene units due to the improved Van der Waals interactions between methylene groups [15].

The X-ray diffractogram given in Fig. 4 shows that before sintering the PA6 and PA12 powders gave reflection peaks at 200 and 002/202, and 100 and 010/110, respectively, at 2 theta at 20° and 23° relating to the alpha phase and 21° relating to the gamma phase [15,16]. The PA6 sintered specimen showed a decrease in the peaks related to the alpha phase and an increase in the peak related to the gamma phase. The gamma phase is not thermodynamically stable in polyamides, being predominant under fast cooling conditions [15–18]. The PA12 sintered specimen gave only a reflection peak at 21° relating to the gamma phase, due to fast thermal exchanges involved in the laser powder sintering.

The micrographs of the specimen surfaces of the PA6/PA12 blends in compositions of 80/20, 50/50 and 20/80 (w/w) are shown in Fig. 5. In the microstructure of the PA6/PA12 specimen with 80/20 composition, the formation of a PA6 co-continuous phase occurred, with particles of PA12 adhered to it. The surface micrographs of the PA6/PA12 specimen in a 50/50 composition also showed the formation of a more porous matrix with a large co-continuous PA6 phase and particles of PA12 adhered.

The surface micrographs of the PA6/PA12 specimen in a 20/80 composition showed higher porosity than the

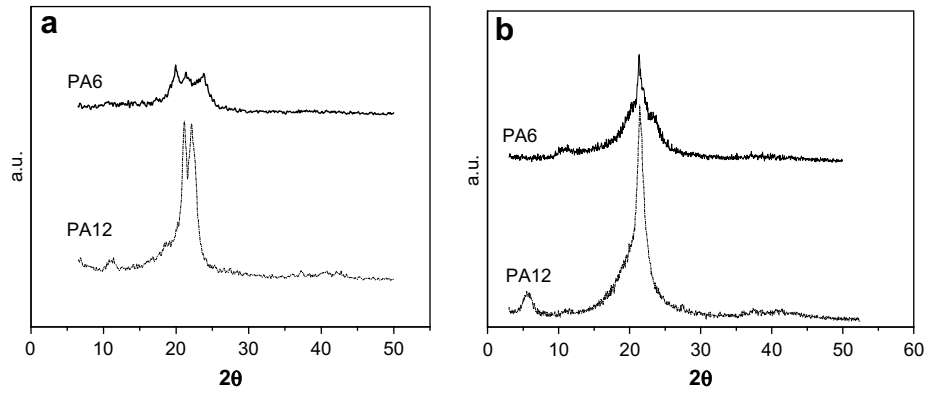

Fig. 4. X-ray diffractograms for PA6 and PA12 powder (a) and specimens (b).

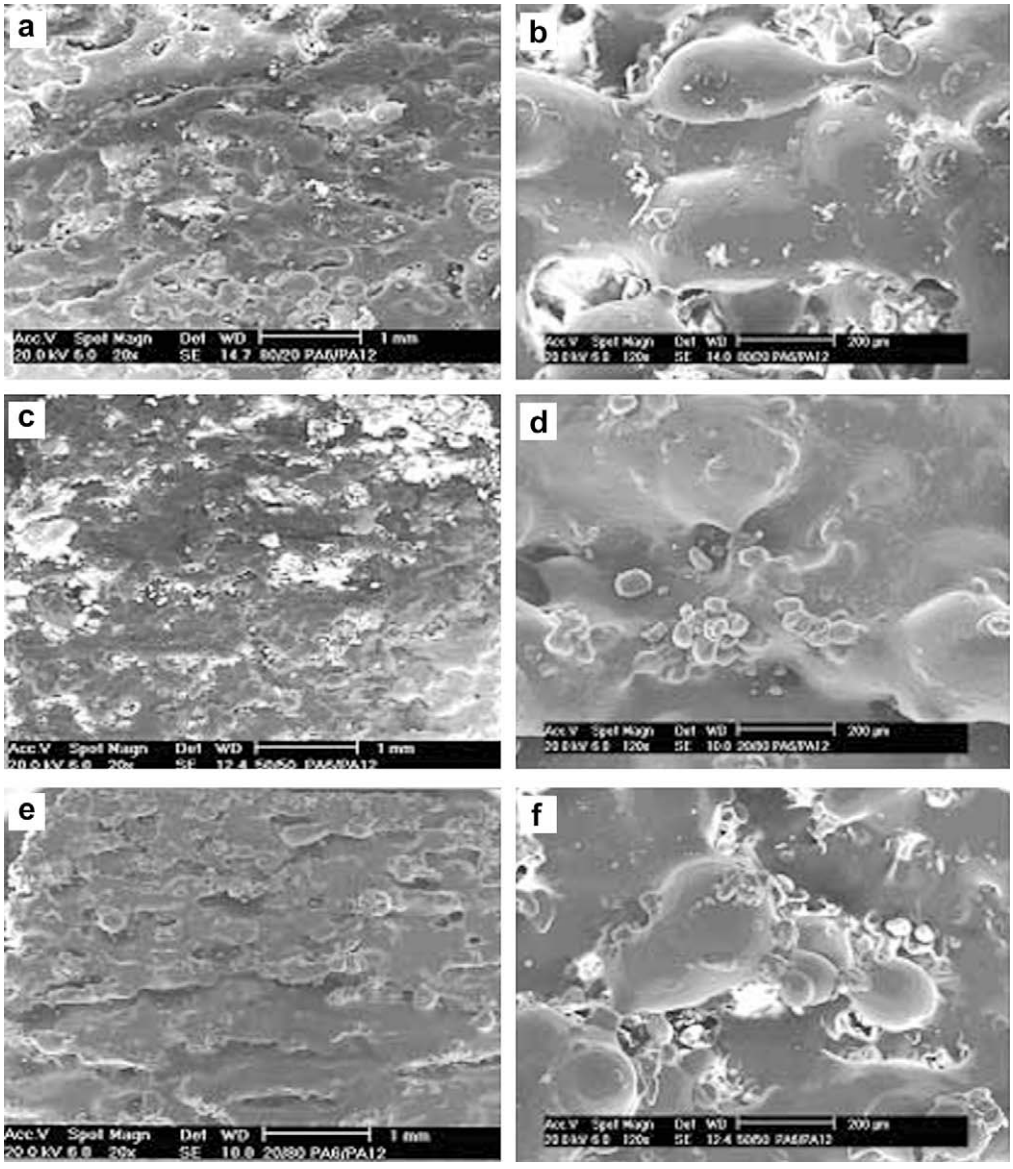

Fig. 5. Surface micrographs for PA6/PA12 specimens: (a) and (b) 80/20 w/w composition, (c) and (d) 50/50 w/w composition, and (e) and (f) 20/80 w/w composition at 20× and 240× magnification, respectively.

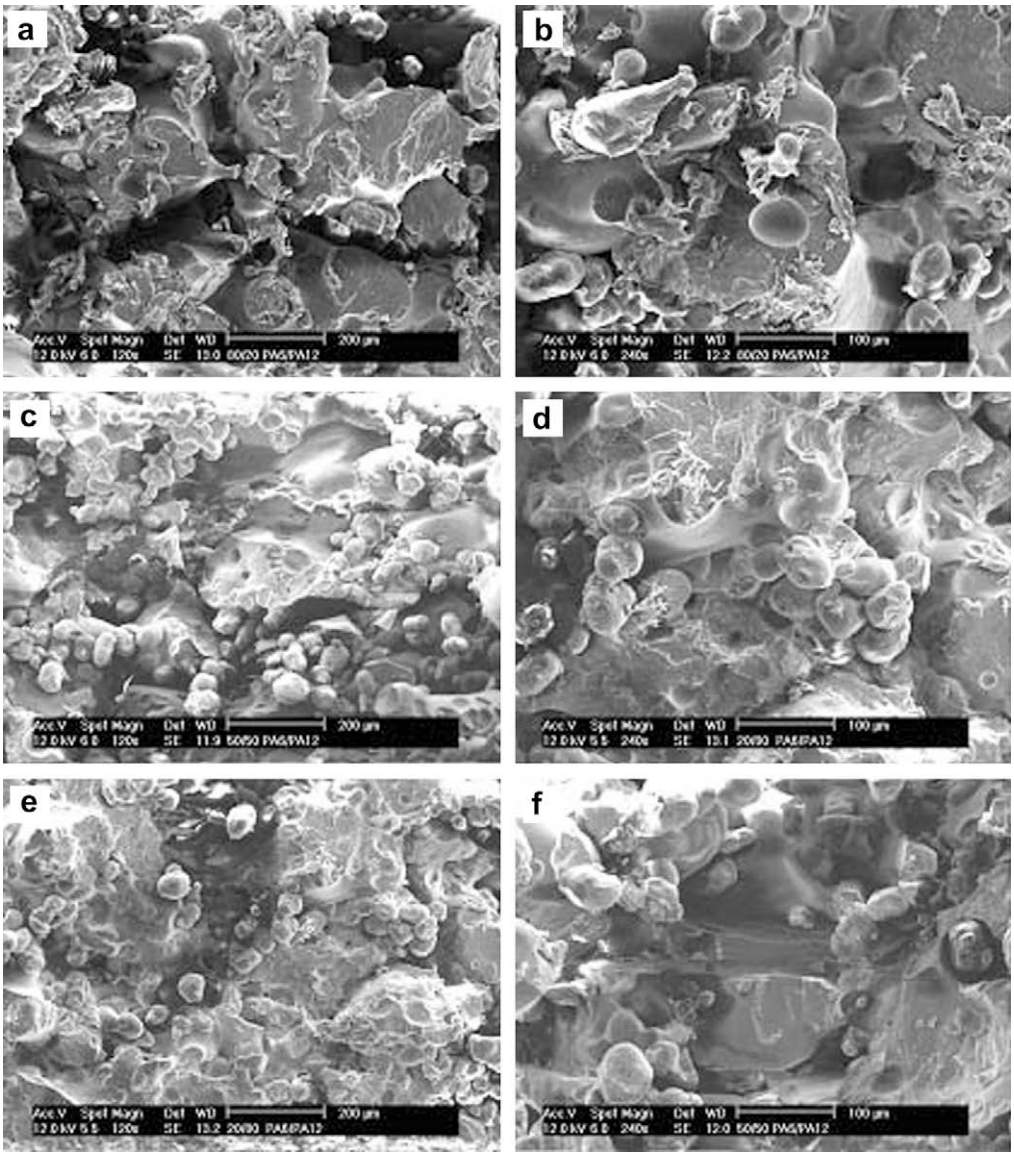

Fig. 6. Cryogenic fracture micrographs of PA6/PA12 specimens: (a) and (b) 80/20 w/w composition, (c) and (d) 50/50 w/w composition, and (e) and (f) 20/80 w/w composition at 20× and 240× magnification, respectively.

specimen in other compositions, due to the low quantity of co-continuous PA6 phase. The PA6 has high laser absorption and a significant melt flow compared to PA12 under the process conditions, as suggested by the MFI values at 200 °C given in Table 1. The results obtained for the PA6/PA12 blends are similar to those reported for PA12/HDPE blends sintered by laser, i.e., the rheologic behavior of the polymeric materials during the process seems to be extremely important in terms of the blend microstructure formation [13].

The fractured surfaces of the PA6/PA12 specimens with compositions of 80/20, 50/50 and 20/80 (w/w) at 120× and 240× magnification are shown in Fig. 6. The 80/20 PA6/PA12 specimen showed microstructure features indicating the existence of PA6 coalescence, large interconnected pores and PA12 particles dispersed in coalescent regions (Fig. 5b). The existence of PA12 domains encapsulated in regions of PA6 coalescence demonstrated the low interaction between the PA6 and PA12 phases. The polyamides present the same chemical function, but a different extension of methylene groups (CH_2) in each chain, resulting in low attraction force and immiscibility in the blend structures.

The 50/50 PA6/PA12 specimen showed low coalescence of the PA6 phase as observed in the surface analysis (Fig. 5c and d). However, the 20/80 PA6/PA12 specimens showed joining of PA12 particles through neck formation and coalescence, which formed a sintered PA12 matrix with pores. This porous microstructure is formed under the moderate viscous flow of PA12.

The DSC curves of PA6/PA12 specimens (Fig. 7) showed melting temperature peaks related to the pure polymers

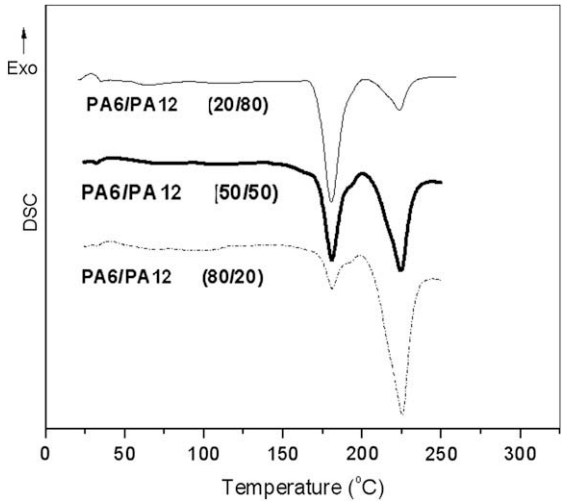

Fig. 7. DSC curves for PA6/PA12 specimens in compositions of 80/20, 50/50 and 20/80 w/w.

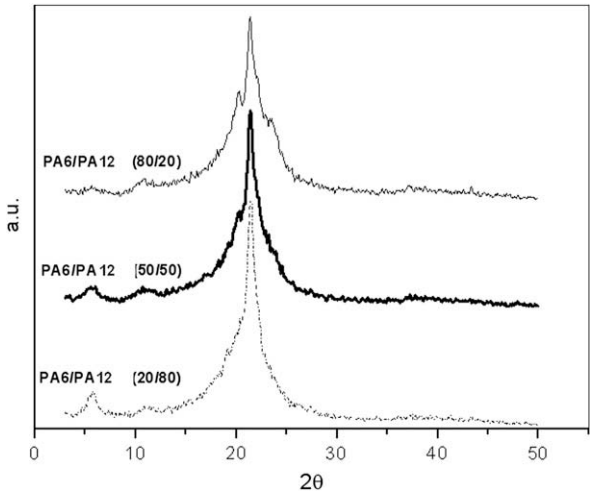

Fig. 8. X-ray diffractograms of PA6/PA12 specimens in compositions of 80/20, 50/50 and 20/80 w/w.

(i.e., PA6 and PA12, 220 and 178 °C, respectively) evidencing the immiscibility in the blends. The DSC peak areas for the polyamides were proportional to the blend composition.

The X-ray diffractograms (Fig. 8) showed that PA6/PA12 blend specimens (80/20, 50/50 and 20/80) give crystalline peaks relating to the PA6 and PA12 gamma phase of the sintered pure materials. The peak intensities were proportional to the blend composition. The presence of the gamma phase is due to the fast thermal exchange involved in selective laser sintering under these conditions.

4. Conclusions

PA6/PA12 blends prepared by SLS show the formation of semi-crystalline microstructures with co-continuous phases and porosities which are dependent on the composition. PA6 has a higher melt flow under the process conditions, resulting in PA6 particle coalescence and co-continuous phase consolidation. The results observed in the PA6/PA12 blend sintering indicate that the rheologic behavior of the polymeric materials during the process seems to be extremely important in terms of the blend microstructure formation. The X-ray diffraction analysis showed that PA6/PA12 blends prepared by SLS give crystalline peaks relating to the polyamide gamma phase due to the fast thermal exchange involved in the blend microstructure formation.

The manufacturing of blends using a selective laser sintering process demonstrated that it is possible to prepare PA6/PA12 blends with controlled structures selecting the polymer powder characteristics, mainly the melt flow behavior. The selective laser sintering of PA6/PA12 blends can permit the development of new applications for SLS technology.

Acknowledgements

The authors would like to thank FAPESC, CAPES, CNPq and FINEP for the financial support.

References

[1] P.F. Jacobs, Rapid Prototyping and Manufacturing: Fundamentals of Stereolithography, Society of Manufacturing Engineers, Dearborn, MI (USA), 1993.
[2] P.F. Jacob, From Rapid Prototyping to Rapid Tooling, ASME, New York, 1999.
[3] D.M. Bourell, H.L. Marcus, J.W. Barlow, J.J. Beaman, Selective laser sintering of metal and ceramics, The International Journal of Powder Metallurgy 28 (1992) 369–382.
[4] K.H. Low, K.F. Leong, C.K. Chua, Z.H. Du, C.M. Cheah, Characterization of SLS parts for drug delivery, Rapid Prototyping Journal 7 (2001) 262–267.
[5] T.H.C. Childs, M. Berzins, G.R. Ryder, A. Tontowi, Selective laser sintering of an amorphous polymer–simulations and experiments, Proceedings of the Institution of Mechanical Engineers 213 (1999) 333–349.
[6] H.C.H. Ho, I. Gibson, W.L. Cheung, Journal of Materials Processing Technology 89 (1999) 204–210.
[7] G.V. Salmoria, C.H. Ahrens, P. Klauss, R.A. Paggi, R.G. Oliveira, A. Lago, Materials Research 10 (2007) 211–214.
[8] EOSINT, Plastic laser-sintering for direct manufacturing. EOS GmgH, Technical Data. Bimingham – UK, 2002. Fine Polyamide PA 2200 for EOSINT P., Material Data Sheet.
[9] Dtm, SLS process and DTM's DuraForm PA, material data sheet. http://www.dtm-corp.com/home.htm.
[10] J. Kim, T.S. Creasy, Selective laser sintering characteristics of nylon 6/clay-reinforced nanocomposite, Polymer Testing 23 (2004) 629–636.
[11] K.H. Tan, C.K. Tha, K.F. Leong, C.M. Heah, P. Cheang, M.S. Abu, S.W. Cha, Biomaterials 24 (2003) 3115–3123.
[12] H. Zheng, J. Zhang, S. Lu, G. Wang, Z. Xu, Materials Letters 60 (2006) 1219–1223.
[13] G.V. Salmoria, J.L. Leite, C.H. Ahrens, A. Lago, A.T.N. Pires, Polymer Testing 26 (2007) 361–368.
[14] G.V. Salmoria, J.L. Leite, R.A. Paggi, A. Lago, A.T.N. Pires, Polymer Testing 27 (2008) 654–659.
[15] R. Androsh, M. Stolp, H.J. Radusch, Simultaneous X-ray diffraction and differential thermal analysis of polymers, Thermochimica Acta 271 (1996) 1–8.
[16] E.D.T. Atkins, M.J. Hill, K. Veluraja, Structural and morphological investigation of nylon 8 chain-folded lamellar crystals, Polymer 36 (1995) 35–42.
[17] M. Mihailova, M. Kresteva, N. Aivazova, V. Krestev, E. Nedkov, Radiation Physics and Chemistry 56 (1999) 581–589.
[18] H. Zarringhalam, N. Hopkinson, N.F. Kamperman, J.J. Vlieger, Material Science and Engineering 435 (2006) 172–180.